GeoScienceWorld
Lithosphere
Volume 2022, Article ID 9949201, 11 pages
https://doi.org/10.2113/2022/9949201

Lithosphere

Research Article

Experimental Investigation on the Effect of Loading and Unloading on Coal Permeability with Different Sediment Beddings

Chaojun Fan,[1,2] **Haiou Wen**,[1] **Hao Sun**,[1] **Lijun Zhou**,[1] **Xinpeng Zhang**,[1] **Chun Zhu**,[3] **and Weiwei Su**[2]

[1]*College of Mining, Liaoning Technical University, Fuxin 123000, China*
[2]*State Key Laboratory of Coal Mine Safety Technology, China Coal Technology & Engineering Group Shenyang Research Institute, Shenyang 113122, China*
[3]*School of Earth Sciences and Engineering, Hohai University, Nanjing 210098, China*

Correspondence should be addressed to Chaojun Fan; chaojunfan@139.com

Received 1 March 2022; Accepted 12 April 2022; Published 30 April 2022

Academic Editor: Xiaoding Xu

Copyright © 2022 Chaojun Fan et al. Exclusive Licensee GeoScienceWorld. Distributed under a Creative Commons Attribution License (CC BY 4.0).

The sediment bedding direction and loading-unloading have significant effect on permeability of coal sample. The coal samples taken from Zhangcun Coal Mine in Shanxi were used to measure coal permeability with different sediment beddings under the effect of loading and unloading by the triaxial coal-rock seepage experimental apparatus. The influence of gas pressure, loading-unloading, and sediment bedding direction on the permeability of coal samples was analyzed, and the functional relationship among these parameters was recovered by fitting. The results show that the permeability of all vertical, dip, and horizontal bedding coal samples decreases exponentially with the increase of effective stress during stress loading, while the permeability of three kinds of bedding coal samples increases exponentially with the decrease of effective stress during stress unloading. Under the same gas pressure, the fracture space of coal samples with vertical and dip bedding is more likely to be compressed and closed at the initial stage of loading, resulting in great decrease of the permeability. In the initial stage of unloading, the microcracks and natural beddings in coals gradually expand and connect. Due to the well development of fractures, the permeability of vertical bedding coal samples increases greatly, while the permeability of dip and horizontal bedding coal samples increases slightly. In the loading process, the permeability of coal sample is vertical bedding > dip bedding > horizontal bedding in order. For the tested samples, the permeability of vertical bedding coal samples is 1.3 to 2.8 times that of dip or horizontal bedding coal samples. In the unloading process, the permeability of the vertical bedding coal samples was 2.8 to 3.3 times that of the dip or horizontal bedding coal samples.

1. Introduction

As a disastrous gas, coal seam gas brings great harm to coal mine production. The permeability in coal seam is the key factor determining the efficiency of gas drainage [1–3]. The mining disturbance will affect the bedding development of fractured coal [4] and thus determine the permeability of coal seam [5–7]. The anisotropy and heterogeneity affect the permeability, which acts an important role in the effective prevention and control of gas disasters [8–12]. Therefore, it is extremely significant to study the variation law of coal permeability with different bedding directions under triaxial loading or unloading.

For the porous material of coal seam, the relationship between coal porosity and permeability is the focused point in the current time, and many conceptual and mathematical models were proposed, including the general porosity-permeability models representing the behavior of coal matrix (primary media) and fractures (secondary media) under variable stress conditions [13], the porosity-permeability model representing the coupling of reservoir and geomechanics [14], and the permeability model representing different

Downloaded from http://pubs.geoscienceworld.org/gsa/lithosphere/article-pdf/doi/10.2113/2022/9949201/5598962/9949201.pdf
by guest

damage zones (caving, fractured, deformed, and original zones) around the longwall face [15]. However, these models did not consider the effect of anisotropy and heterogeneity on coal permeability. With the deepening research of coal permeability, some scholars put forward an improved anisotropic permeability model through the finite element method [16, 17] and studied the effect of permeability heterogeneity on the production of coalbed methane [18, 19]. Based on the principle of equivalent displacement, Lin et al. [20] described the permeability of anisotropic coal in different directions and established a structural anisotropy and multiphysical field coupling model for gas-bearing coal seams. After the same time period of gas drainage, the residual gas concentration in the coal seam when the borehole is perpendicular to the bedding direction is about 1.4 times that in the parallel bedding direction. Hence, the drilling arrangement is suggested to be perpendicular to the bedding direction of coal seam. Ma et al. [21] and Fan et al. [22] studied the relationship between the anisotropic permeability and fracture structure of coal samples in three directions, and the results show that microfractures are crucial to the permeability parallel to the bedding direction, which leads to a higher anisotropy ratio between parallel and perpendicular to the bedding direction.

Scholars also carried out investigation on the seepage properties of coal and rock mass by series of physical experiments. The permeability model for shale under anisotropic true triaxial stress conditions has been established through the self-developed triaxial seepage instrument for testing the seepage properties [23, 24]. Some scholars considered the influence of coal bedding and stress state on permeability and proposed a layer-based permeability model [25] and dynamic anisotropy (*D-a*) permeability model [26]. Liu et al. [27] and Li et al. [28] carried out the experiments on the coal deformation and permeability evolution under the condition of true triaxial stress and established the stress-strain relationship model of bedding coal to quantify the influence of bedding effect on coal permeability under the triaxial stress state. The deformation of coal is closely similar to the deformation of shale bedding, and the stress path and effective confining stress on coal have significant influences on its deformation behavior and permeability evolution [29–31]. In addition, stress loading and unloading conditions have a significant effect on the permeability of bedding coal. For example, in the process of deep mining, the excavation disturbance stress path [32], confining pressure [33], bedding structure [34, 35], gas temperature and pressure, creep stress, and strain have significant influence on gas seepage law [36, 37]. Under the same unloading condition, the increase of permeability of coal samples with parallel bedding fractures is much larger than that of coal samples with vertical bedding fractures [38]. Under layered cyclic loading, the gas slip effect is greater than the effective stress effect in the low pore gas pressure range [39–41]. It is found that the permeability of coal reservoir in different directions decreases exponentially with the increase of effective stress [42, 43]. Wang et al. [44] and Fan et al. [45] proposed an analytical model to describe the anisotropic permeability evolution of coal due to the change of effective stress and gas adsorption, which captures various effects of mechanical properties and gas adsorption-induced directional strains on anisotropic characteristics.

However, the evolution law of permeability of coal samples with different bedding directions under loading and unloading conditions requires further studies. In this paper, the seepage experiments on coal samples with three types of beddings, vertical, dip, and horizontal, under the constant gas pressure, and varying loading-unloading conditions were carried out, by using the triaxial stress coal-rock seepage experimental apparatus. The influence of effective stress on coal permeability is studied to provide a reference for safe and efficient gas drainage during coal mining.

2. Experimental Apparatus and Scheme

2.1. Coal Sample Preparation. Coal blocks with layered sediment structure were collected from the 2606 roadway (3# coal seam) in Zhangcun Coal Mine, Shanxi Province. Coal samples with horizontal bedding at natural moisture content (HN, horizontal-natural), vertical bedding (VN, vertical-natural), and dip bedding (DN, dip-natural) were drilled out by a rock drilling sampler from the collected coal block, and the samples were processed to be 50 mm × 100 mm (diameter × height) in size, with the flatness of ±0.05 mm at the end faces. Each bedding form has a group of 3 coal samples marked as 1#, 2#, and 3#, respectively. As shown in Figure 1, the angle between the radial direction of coal sample and the bedding is defined as β; thus, the horizontal bedding and the vertical bedding are $\beta = 0^\circ$ and $\beta = 90^\circ$. The dip samples are DN-1# ($\beta = 39^\circ$), DN-2# ($\beta = 45^\circ$), and DN-3# ($\beta = 42^\circ$). In order to minimize the manual error in processing and the individual divergence of coal samples, experiments were carried out on the same group of coal samples placed in a holder after applying a uniform silicone rubber around.

2.2. Experimental Apparatus and Principle. The experiments on the permeability of coal samples under loading and unloading conditions were carried out by the triaxial stress coal-rock seepage experimental apparatus at Liaoning Technical University, as shown in Figure 2. The experimental apparatus is mainly composed of seven parts: hydraulic servo loading unit, clamping device, constant temperature unit, gas supply unit, gas pressure control unit, data acquisition and analysis unit, and auxiliary unit, e.g., pipelines.

Figure 3 shows the principle of the triaxial stress coal-rock seepage experimental apparatus. The hydraulic servo loading unit includes a ring pressure tracking pump, a pressure gauge, and an axial stress pump, which can adjust the confining and axial stress on coal sample. The processed coal sample is put into the holder, and the temperature in the experiment can be adjusted by the incubator. The gas supply unit includes a nitrogen cylinder and pressure-reducing valve. The gas pressure control unit includes gas booster pump, air compressor, automatic pressure switch, pressure gauge, storage tank, pressure-regulating valve, and pressure sensor. Nitrogen gas is stored in the storage tank through the gas booster pump, and the pressure-regulating valve

Downloaded from http://pubs.geoscienceworld.org/gsa/lithosphere/article-pdf/doi/10.2113/2022/9949201/5598962/9949201.pdf
by guest

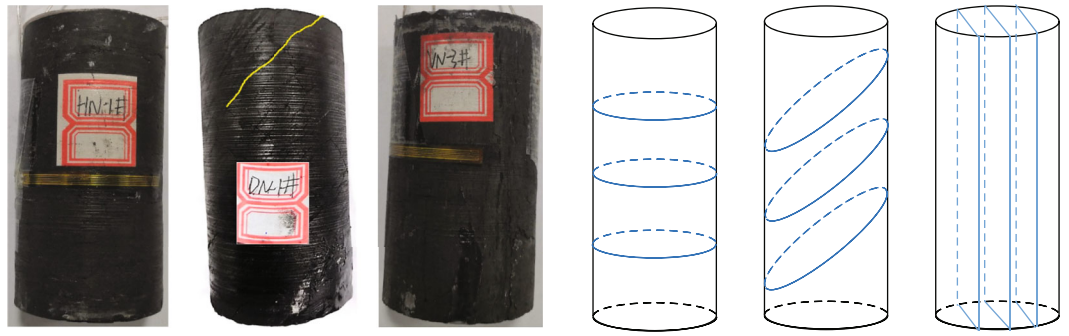

Figure 1: Prepared coal samples with different beddings. (a) Photo of the prepared coal sample. (b) Sketch of the bedding direction in the fractured coal.

Figure 2: Photo of the triaxial stress coal-rock seepage experimental apparatus.

can adjust the gas pressure. The flowmeter can detect the gas flow rate and gas flow. The sensor data monitored from the confining stress tracking pump, flowmeter, and pressure are transmitted to the computer through the data bus for storage, analysis, and processing.

The experiments on different bedding coal samples were carried out by changing the injected gas pressure, while the triaxial stress of loading and unloading is applied to the coal samples. The average effective stress can be calculated according to the following:

$$\sigma = \frac{1}{3}(\sigma_1 + 2\sigma_2) - \frac{1}{2}(P_1 - P_2), \tag{1}$$

where σ is the average effective stress (MPa); σ_1 is the axial stress (MPa); σ_2 is the confining stress (MPa); P_1 is the inlet gas pressure (MPa); P_2 is the outlet gas pressure (MPa), which is equal to the atmospheric pressure in this study.

Assume that the nitrogen migration in coal sample is an isothermal process, and the nitrogen seepage conforms to Darcy's law. The permeability of coal sample during the loading and unloading failure is calculated by the following:

$$k = \frac{2\mu P_0 QL}{A_s\left(P_1^2 - P_2^2\right)}, \tag{2}$$

where k is the permeability of coal sample (mD); μ is the viscosity coefficient of methane (Pa·s); P_0 is the atmospheric pressure of measuring point (MPa); P_1 and P_2 are the gas pressures at the inlet and outlet of the holder (MPa); Q is the nitrogen flow rate at a standard condition (cm^3/s); L is the length of coal sample (cm); A_s is the cross-sectional area of the coal sample (cm^2).

2.3. Experimental Scheme. In the seepage experiment, the initial axial stress is set as 5 MPa, and the initial confining stress is set as 4 MPa, as shown in Figure 4. We adopt the step loading scheme of axial and circular pressure at the same time; that is, the axial stress gradient is 2.5 MPa and the circular pressure gradient is 2 MPa. For the stress unloading experiment, the initial axial stress is 20 MPa, and the initial confining stress is 16 MPa. We adopt the axial stress as a constant of 20 MPa and the confining stress as a step unloading scheme, with the confining stress gradient of 0.5 MPa. Inlet pressure is set as 1 or 2 MPa, and outlet pressure is set as 0.1 MPa—atmospheric pressure.

Downloaded from http://pubs.geoscienceworld.org/gsa/lithosphere/article-pdf/doi/10.2113/2022/9949201/5598962/9949201.pdf
by guest

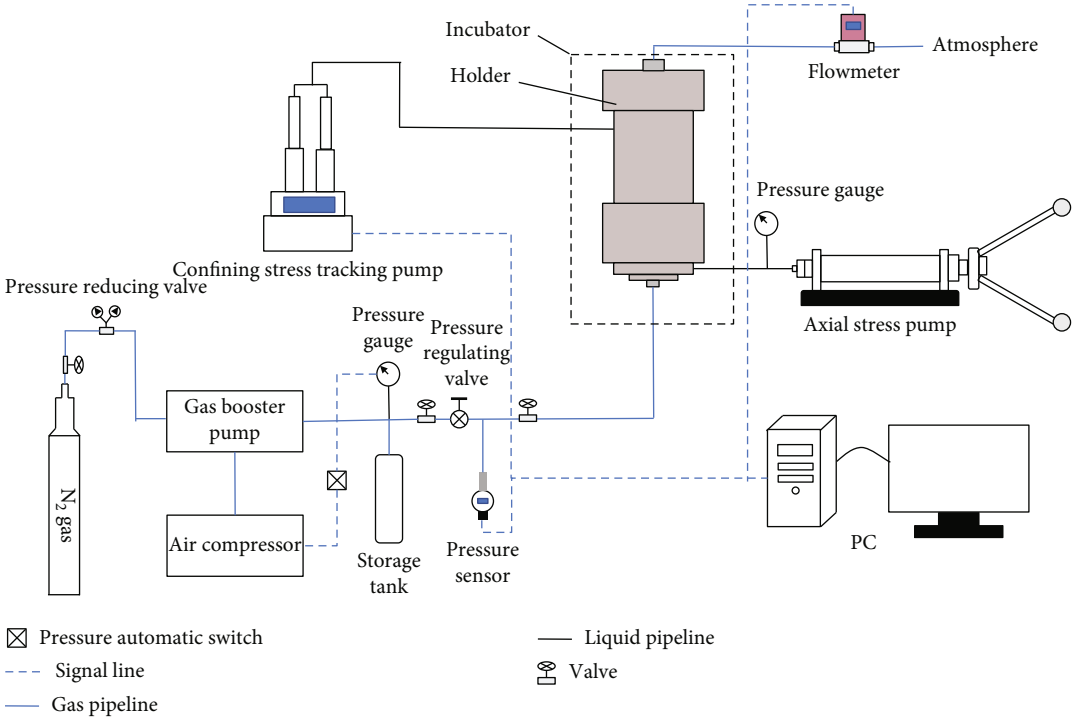

Figure 3: Principle of the triaxial stress coal-rock seepage experimental apparatus.

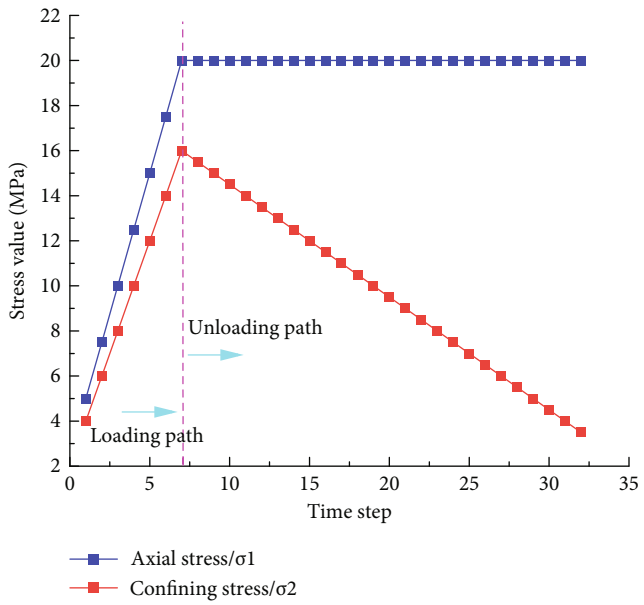

Figure 4: Stress loading and unloading scheme.

The specific steps of the seepage experiments are as follows:

(1) The longitudinal and transverse strain gauges are pasted on the surface of coal sample with glue to ensure the firmness

(2) Put coal sample with strain gauge into the holder, connect the signal line of strain gauge to the strain monitor, and check whether the strain signal can be transmitted to the computer successfully

(3) Install the lower base of the holder, align the upper and lower bases of the holder, tighten the bolts, and seal with a sealing ring. Connect relevant pipelines and instruments, empty the filled water, and test the air tightness of the apparatus

(4) Stress loading step: close the liquid outlet valve and start the computer loading control program. Apply axial stress of 5 MPa and radial pressure (confining stress) of 4 MPa on the coal sample through the hydraulic loading unit. Inject gas into coal sample with a certain pressure to obtain the initial pressure in coal sample. The confining stress should be slightly greater than the injected gas pressure to ensure the stability and air tightness of coal sample. This avoids nitrogen gas flowing through the edge of the holder. In the process of stress loading, the axial stress and the confining stress are increased simultaneously. Specifically, the axial stress is adjusted from 5 MPa to 20 MPa with an increase pressure gradient of 2.5 MPa, and the confining stress is adjusted from 4 MPa to 16 MPa with an increase pressure gradient of 2 MPa. Adjust the gas outlet valve of the high-pressure gas cylinder to maintain the tested gas pressure as schemed in Figure 4

(5) Stress unloading step: after the nitrogen gas is balanced, the radial pressure and the axial stress are 16 MPa and 20 MPa, respectively. Keep the axial stress constant and gradually unload the confining stress with a decrease gradient of 0.5 MPa until the

Downloaded from http://pubs.geoscienceworld.org/gsa/lithosphere/article-pdf/doi/10.2113/2022/9949201/5598962/9949201.pdf
by guest

Table 1: Permeability tested results of different bedding coal samples during the loading process.

Gas pressure of 1 MPa				Gas pressure of 2 MPa		
Effective stress (σ/MPa)	Permeability (K/mD)			Effective stress (σ/MPa)	Permeability (K/mD)	
	VN-1/90°	DN-1/39°	HN-1/0°		DN-3/42°	HN-2/0°
3.88		0.755	0.652	3.38	0.334	0.298
6.05	1.050	0.494	0.493	5.55	0.239	0.217
8.22	0.753	0.314	0.462	7.72	0.151	0.134
10.38	0.501	0.212	0.422	9.88	0.105	0.091
12.55	0.363	0.145	0.120	12.05	0.075	0.066
14.72	0.271	0.102	0.087	14.22	0.057	0.051
16.88	0.206	0.074	0.063	16.38	0.043	0.040

confining stress is slightly greater than the injected gas pressure as schemed in Table 1. During unloading, the pressure sensor measures the injected gas pressure, and the flowmeter collects the gas flow rate and flow flux

(6) Replace coal sample, change the injected gas pressure, and repeat the above steps

3. Results and Discussions

3.1. Effect of the Effective Stress on Coal Permeability during Loading. For the seepage experiment in loading step, both the axial stress and the confining stress are synchronous loaded. The axial stress is adjusted from 5 MPa to 20 MPa with an increase pressure gradient of 2.5 MPa, and the confining stress is adjusted from 4 MPa to 16 MPa with an increase pressure gradient of 2 MPa. The confining stress is slightly larger than that of injected gas pressure, as shown in Table 1.

Figure 5(a) shows the evolution of permeability of different bedding coal samples under the conditions of injected gas pressure of 1 MPa, the initial axial stress of 5 MPa, and initial confining stress of 4 MPa. As the loaded effective stress increases from 6.05 MPa to 10.38 MPa, the permeability of vertical sample VN-1# decreases from 1.050 mD to 0.501 mD in an exponential function, the permeability of dip sample DN-1# exponentially decreases from 0.494 mD to 0.212 mD, and the permeability of horizontal sample HN-1# exponentially decreases from 0.493 mD to 0.422 mD. The permeability decreased by 52.29%, 57.0%, and 14.4% for vertical, dip, and horizontal bedding coal samples, respectively.

Figure 5(b) shows the variation of the permeability of different bedding coal samples with the injected gas pressure of 2 MPa, the initial axial stress of 5 MPa, and the initial confining stress of 4 MPa. The bedding angles β of DN-3# and HN-2# are 42° and 0°, respectively. As the loaded effective stress increases from 3.38 MPa to 5.55 MPa, the permeability of dip sample DN-3# exponentially decreases from 0.334 mD to 0.239 mD, and the permeability of horizontal sample HN-2# exponentially decreases from 0.298 mD to 0.217 mD. The permeability decreased by 28.44% and 27.18% for dip and horizontal samples, respectively. It can be implied that the fracture space of vertical and dip samples is easier to be compressed and closed than that of horizontal bedding coal samples at the initial stage, resulting in greater decrease of the permeability.

The exponential function is selected for fitting, and the formula is as follows:

$$k = Ae^{B\sigma}, \tag{3}$$

where σ is the average effective stress (MPa); A and B are the fitting coefficients.

The curves of permeability of different bedding coal samples with the average effective stress were fitted during the loading process in Figure 5.

From Equation (1), the average effective stresses of vertical, dip, and horizontal bedding coal samples are the same when the same axial stress and confining stress are loaded under the constant injected gas pressure, and the pressure gradient of each step is the same. Furthermore, the variation trend and magnitude of coal permeability with average effective stress were compared. Figure 5(a) shows the fitting curves of permeability of vertical sample VN-1# ($\beta = 90°$), dip sample DN-1# ($\beta = 39°$), and horizontal sample HN-1# ($\beta = 0°$) with average effective stress during loading when the injected gas pressure is 1 MPa; the coefficients of these fitted exponential functions are 0.997, 0.99866, and 0.84189, respectively. Figure 5(b) shows the fitting curves of permeability of dip sample DN-3# ($\beta = 42°$) and horizontal sample HN-2# ($\beta = 0°$) with average effective stress during loading when the injected gas pressure is 2 MPa; the coefficients of these fitted exponential functions are 0.99597 and 0.99351, respectively. With the continuous increase of the average effective stress, there is a minimum point in the decreasing coal permeability. The coal sample undergoes compaction, including both elastic and plastic deformations, leading to the final permeability which tends to be a stable minimum value [46, 47].

When the axial stress is 5 MPa, confining stress is 4 MPa, and the injected gas pressure is 1 MPa. The initial permeability of vertical sample VN-1# ($\beta = 90°$) is 1.3 times that of dip sample DN-1# ($\beta = 39°$), as shown in Figure 6(a). With gradual increase of the average effective stress, the maximum and minimum permeability ratio of VN-1# to DN-1# are 2.8 and 1.3, respectively. The initial permeability of vertical sample VN-1# ($\beta = 90°$) is 1.5 times that of horizontal sample HN-

Downloaded from http://pubs.geoscienceworld.org/gsa/lithosphere/article-pdf/doi/10.2113/2022/9949201/5598962/9949201.pdf
by guest

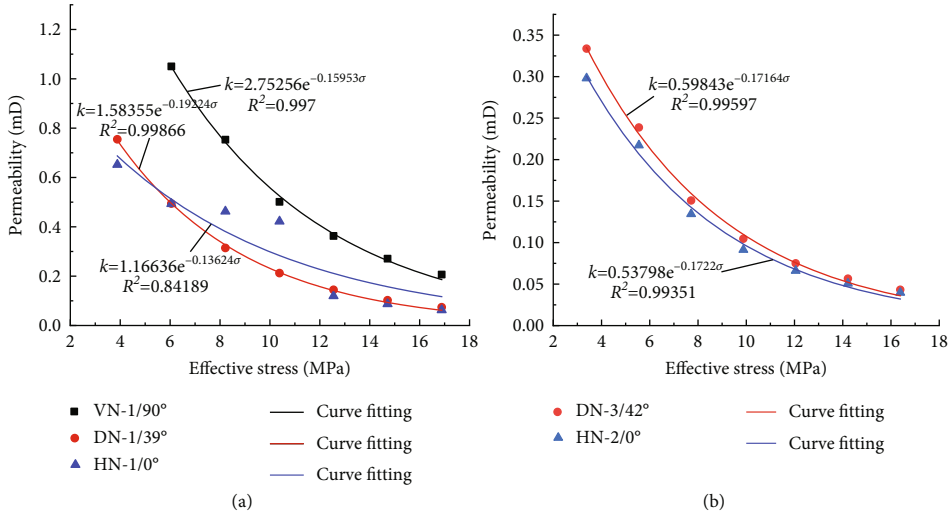

FIGURE 5: Permeability change of different bedding coal samples during stress loading. (a) Gas pressure of 1 MPa. (b) Gas pressure of 2 MPa.

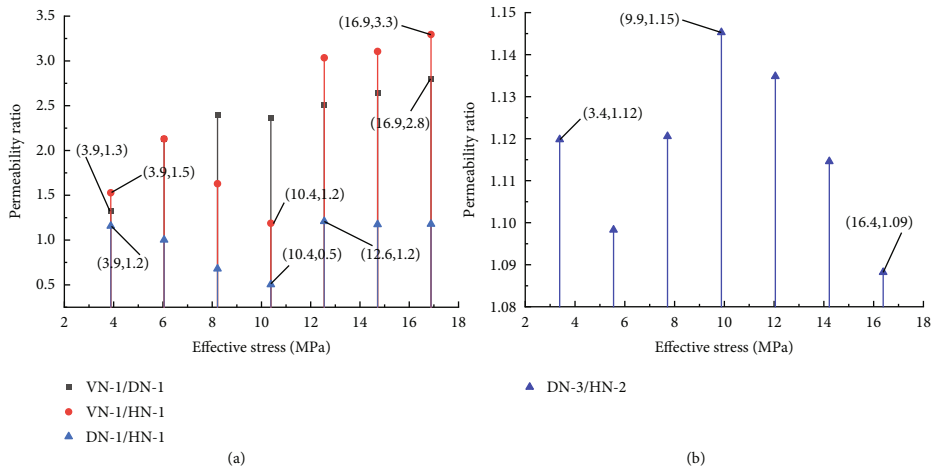

FIGURE 6: Permeability ratios of different bedding coal samples during stress loading. (a) Gas pressure of 1 MPa. (b) Gas pressure of 2 MPa.

1# ($\beta = 0°$). With a gradual increase of the average effective stress, the maximum and minimum permeability ratios of coal samples VN-1# to HN-1# are 3.3 and 1.2, respectively. The initial permeability of the dip sample DN-1# ($\beta = 39°$) is 1.2 times that of the horizontal sample HN-1# ($\beta = 0°$). With the increase of the average effective stress, the maximum and minimum permeability ratios of DN-1# to HN-1# coal sample are 1.2 and 0.5, respectively.

Figure 6(b) presents permeability ratios of different bedding coal samples during loading when the injected gas pressure is 2 MPa. The initial permeability of the dip sample DN-3# ($\beta = 42°$) is 1.12 times that of the horizontal sample HN-2# ($\beta = 0°$). With the increase of average effective stress, the permeability ratio of coal samples DN-3# to HN-2# is featured by a maximum value of 1.15 and a minimum value of 1.09.

3.2. Effect of the Effective Stress on Coal Permeability during Unloading. In the unloading step of seepage experiment, the axial stress remained unchanged -20 MPa, and the confining stress is unloaded in steps from 16 MPa to 3.5 MPa with 0.5 MPa/step. The confining stress should be slightly larger than the injected gas pressure. When the injected gas pressure is 1 or 2 MPa, the permeability of the different bedding coal samples increases exponentially with the decrease of the effective stress in the process of unloading, as shown in Table 2.

When the gas pressure is 1 MPa and the effective stress is 16.88 MPa, the initial permeabilities of coal samples VN-1#, DN-1#, and HN-1# are 0.206 mD, 0.074 mD, and 0.063 mD, respectively. As the unloaded effective stress decreases from 16.88 MPa to 15.55 MPa, the permeability of coal sample VN-1# is 104.85% of the initial value, the permeability of the dip sample DN-1# does not change, and the permeability of coal sample HN-1# is 104.76% of the initial value. When the effective stress is unloaded to 13.55 MPa, this ratio becomes 122.82%, 112.16%, and 128.57% for vertical, dip, and horizontal samples, respectively.

When the gas pressure is 2 MPa and the effective stress is 16.38 MPa, the initial permeabilities of coal samples DN-3#

Downloaded from http://pubs.geoscienceworld.org/gsa/lithosphere/article-pdf/doi/10.2113/2022/9949201/5598962/9949201.pdf
by guest

Table 2: Permeability of different bedded coal samples under the same gas pressure during unloading.

Gas pressure of 1 MPa				Gas pressure of 2 MPa		
Effective stress (σ/MPa)	Permeability (K/mD)			Effective stress (σ/MPa)	Permeability (K /mD)	
	VN-1/90°	DN-1/39°	HN-1/0°		DN-3/42°	HN-2/0°
16.88	0.206	0.074	0.063	16.38	0.043	0.040
16.55	0.205	0.072	0.062	16.05	0.043	0.038
16.22	0.208	0.072	0.064	15.72	0.044	0.040
15.88	0.213	0.073	0.066	15.38	0.045	0.040
15.55	0.216	0.074	0.066	15.05	0.046	0.041
15.22	0.221	0.076	0.069	14.72	0.047	0.042
14.88	0.228	0.078	0.070	14.38	0.048	0.043
14.55	0.235	0.080	0.072	14.05	0.050	0.045
14.22	0.241	0.081	0.074	13.72	0.051	0.046
13.88	0.251	0.081	0.077	13.38	0.053	0.048
13.55	0.253	0.083	0.081	13.05	0.055	0.050
13.22	0.253	0.086	0.085	12.72	0.057	0.052
12.88	0.273	0.084	0.089	12.38	0.059	0.055
12.55	0.281	0.090	0.093	12.05	0.061	0.057
12.22	0.295	0.093	0.098	11.72	0.065	0.060
11.88	0.312	0.097	0.105	11.38	0.068	0.064
11.55	0.330	0.099	0.111	11.05	0.072	0.069
11.22	0.347	0.104	0.119	10.72	0.076	0.074
10.88	0.370	0.109	0.130	10.38	0.081	0.080
10.55	0.393	0.114	0.143	10.05	0.089	0.086
10.22	0.392	0.117	0.159	9.72	0.097	0.096
9.88	0.417	0.126	0.177	9.38	0.107	0.106
9.55	0.451	0.136	0.202	9.05	0.117	0.117
9.22	0.489	0.148	0.237	8.72	0.123	0.132
8.88	0.529	0.163	0.283	8.38	0.135	0.148
8.55	0.595	0.182	0.353	8.05	0.155	0.173

and HN-2# are 0.043 mD and 0.040 mD, respectively. As the effective stress is unloaded from 16.38 MPa to 15.05 MPa, the permeability of the dip sample DN-3# is 106.97% of the initial value, and the permeability of the horizontal sample HN-2# is 102.5% of that initial value. When the effective stress is unloaded to 13.05 MPa, this ratio becomes 127.90% and 125% for dip and horizontal samples, respectively.

During the unloading process, the axial stress remains unchanged, the confining stress decreases, and the microcracks and beddings in the coal sample expand and connect. Due to the well development of fractures in the vertical sample, there exist many gas seepage channels. The permeability of the vertical samples increases significantly, while the permeability of dip and the horizontal samples increases slightly.

As shown in Figure 7, the change curves of permeability of different bedding coal samples under constant gas pressure with the decrease of average effective stress were fitted. Figure 6(a) presents the fitting curves of permeability of vertical sample VN-1# ($\beta = 90°$), dip sample DN-1# ($\beta = 39°$), and horizontal sample HN-1# ($\beta = 0°$) with average effective stress during unloading when the gas pressure is 1 MPa. The permeabilities of coal samples VN-1# ($\beta = 90°$), DN-1# ($\beta = 39°$), and HN-1#($\beta = 0°$) show an exponential increase in the process of decreasing average effective stress. The exponential function is fitted as shown in Figure 7(a), and the coefficients of these fitted exponential functions are 0.95154, 0.89286, and 0.9001, respectively.

Figure 7(b) shows the fitting curves of permeability of dip sample DN-3#($\beta = 42°$) and horizontal sample HN-2# ($\beta = 0°$) with average effective stress during unloading process when the gas pressure is 2 MPa; the coefficients of these fitted exponential functions are 0.94625 and 0.93685, respectively. Dip sample DN-3# ($\beta = 42°$) and horizontal sample HN-2# ($\beta = 0°$) also show an exponential increase in permeability during the decreasing of average effective stress. The exponential function is fitted as shown in Figure 7(b).

Hence, the exponential function can be used to express the influence of effective stress on coal permeability under constant gas pressure during stress unloading.

In Figure 8(a), when the axial stress, confining stress, and gas pressure are 20 MPa, 16 MPa, and 1 MPa, respectively, the initial permeability of vertical sample VN-1# ($\beta = 90°$) is 2.8 times that of dip sample DN-1# ($\beta = 39°$).With the

Downloaded from http://pubs.geoscienceworld.org/gsa/lithosphere/article-pdf/doi/10.2113/2022/9949201/5598962/9949201.pdf
by guest

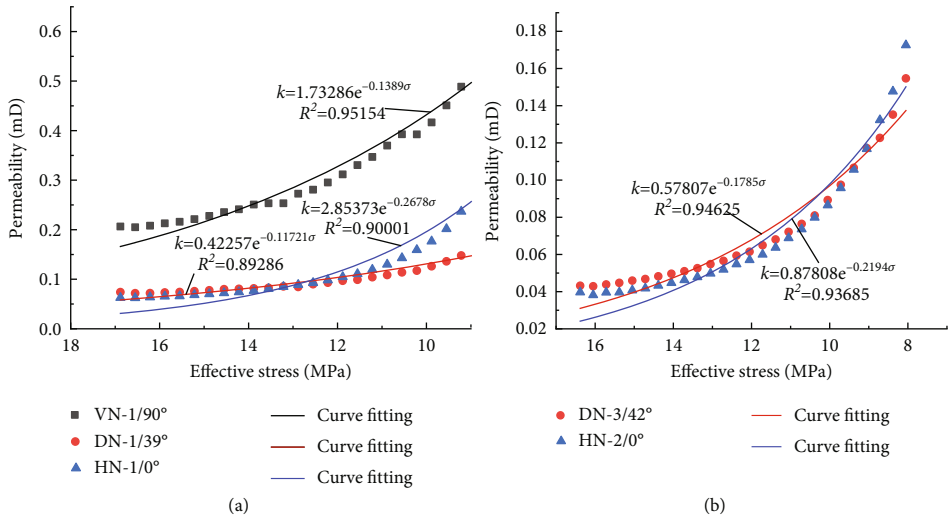

FIGURE 7: Permeability change of different bedding coal samples during stress unloading. (a) Gas pressure of 1 MPa. (b) Gas pressure of 2 MPa.

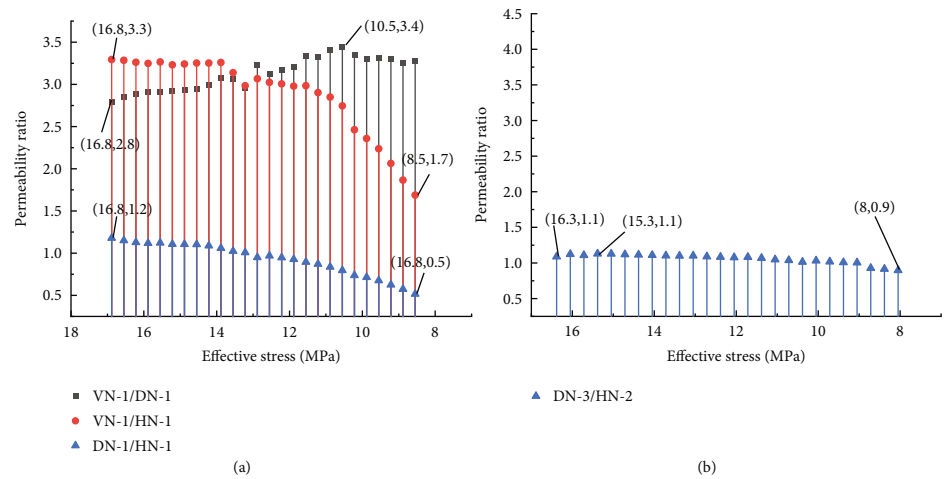

FIGURE 8: Permeability ratios of different bedding coal samples during stress unloading. (a) Gas pressure of 1 MPa. (b) Gas pressure of 2 MPa.

gradual decrease of the average effective stress, the maximum and minimum permeability ratios of coal samples VN-1# to DN-1# are 3.4 and 2.8, respectively. The initial permeability of vertical sample VN-1# ($\beta = 90°$) is 3.3 times that of horizontal sample HN-1# ($\beta = 0°$). With the decrease of the average effective stress, the maximum and minimum permeability ratios of VN-1# to HN-1# are 3.3 and 1.7, respectively. The initial permeability of the dip sample DN-1# ($\beta = 39°$) is 1.2 times that of the horizontal sample HN-1# ($\beta = 0°$). With the gradual decrease of the average effective stress, the maximum and minimum permeability ratios of DN-1# to HN-1# are 1.2 and 0.5, respectively. In Figure 8(b), when the axial stress, confining stress, and gas pressure are 20 MPa, 16 MPa, and 2 MPa, the initial permeability of dip sample DN-3# ($\beta = 42°$) is 1.1 times that of horizontal sample HN-2# ($\beta = 0°$).With the gradual decrease of the average effective stress, the maximum and minimum permeability ratios of coal samples DN-3# to HN-2# are 1.1 and 0.9, respectively.

When the gas pressure is 1 or 2 MPa, the overall and initial permeabilities of the vertical samples during the stress unloading are 2.8 to 3.3 times that of the dip or horizontal samples during stress unloading. The permeability of vertical samples is always higher than that of dip and horizontal samples, as shown in Figure 8(a). When the gas pressure is 2 MPa, the permeabilities of the dip and horizontal samples are similar, as shown in Figure 8(b). In the unloading process, the fracture space in coal sample extends and expands passively, instead of the compression of fracture under stress loading. The microcracks and beddings in the coal sample gradually connect, the number of gas permeation channels increases, and the rate of gas transport within coal becomes faster. The difficulty of gas permeation is closely related to the direction of fissures and beddings in coal seam. The

Downloaded from http://pubs.geoscienceworld.org/gsa/lithosphere/article-pdf/doi/10.2113/2022/9949201/5598962/9949201.pdf
by guest

fracture network of vertical and dip bedding coal samples is greatly developed, and the porosity in coal is large to promote gas penetrating in the bedding direction more easily. For the horizontal samples, the coal matrix hinders the seepage ability of gas leading to a smaller permeability. The change curves of permeability of vertical, horizontal, and dip samples with average effective stress in the unloading process decrease exponentially.

The permeabilities of vertical, dip, and horizontal samples decrease exponentially with the increase of effective stress during stress loading, and the permeabilities of three bedding coal samples increase exponentially with the decrease of effective stress during stress unloading. In the process of stress loading and unloading, the change trend of permeability with effective stress is opposite.

4. Conclusions

In this paper, coal samples with three kinds of beddings, vertical, dip, and horizontal, are subjected to triaxial seepage experiments under loading and unloading steps to analyze the evolution law of permeability of coal samples with different bedding directions. The conclusions are drawn:

(1) When the gas pressure is 1 or 2 MPa, the permeability of coal samples decreases exponentially with the increase of effective stress during stress loading, no matter the bedding is in vertical, dip, or horizontal direction. Meanwhile, in process of stress unloading, the permeability of all coal samples increases exponentially with the decrease of the effective stress

(2) Under the same gas pressure, at the initial stage of stress loading, the fracture space of vertical and dip bedding coal samples is more likely to be compacted and closed than that of horizontal samples, and thus, the permeability decreases greatly. In the initial unloading stage, the microfractures and natural fractures in the coal sample gradually expand and connect. The well development of fractures in the vertical sample provides many gas seepage channels to increase the permeability greatly, while the permeability of dip and horizontal samples increases slightly

(3) During stress loading, the initial permeability of vertical sample is 1.3 times that of dip sample and 1.5 times that of horizontal sample. The initial permeability of dip sample is 1.2 times that of the horizontal sample. The initial permeabilities are vertical bedding > dip bedding > horizontal bedding in order. The permeability of vertical samples is generally 1.3 to 2.8 times that of dip or horizontal samples, while the permeability of dip samples is partially larger than that of horizontal samples. During stress unloading, the initial and overall permeability of vertical samples is 2.8 to 3.3 times that of dip or horizontal samples, while the initial and overall permeabilities of dip and horizontal samples are similar

In the future, anisotropic permeability tests of coal samples with different metamorphic degrees will be carried out considering acoustic emission and temperature effects. In addition, the type and adsorption characteristics of injected gas also act a significant role in coal permeability; thus, relevant research will also be carried out.

Data Availability

The data is obtained using the triaxial stress coal-rock seepage experimental apparatus in Liaoning Technical University. The data can be available by contacting the corresponding author if required.

Conflicts of Interest

The authors declare no competing financial interest.

Acknowledgments

This research was financially supported by the National Natural Science Foundation of China (Grant Nos. 52174117, 52004117, and 52074146), the Natural Science Foundation of Liaoning Province (Grant No. 2020-KF-13-05), the Basic Research Project of Liaoning Provincial Education Department (Grant No. LJ2020JCL005), the project supported by the Postdoctoral Science Foundation of China (Grant Nos. 2021T140290 and 2020M680975), and the project supported by the discipline innovation team of Liaoning Technical University (Grant No. LNTU20TD-03).

References

[1] C. J. Fan, L. Yang, G. Wang, Q. M. Huang, X. Fu, and H. O. Wen, "Investigation on coal skeleton deformation law in CO_2 injection enhanced CH_4 drainage from underground coal seam," *Frontiers in Earth Science*, vol. 9, article 891, 2021.

[2] Y. Song, B. Jiang, M. Li, C. L. Hou, and S. C. Xu, "A review on pore-fractures in tectonically deformed coals," *Fuel*, vol. 278, article 118248, 2020.

[3] B. Xiao, S. Liu, Z. W. Li et al., "Geochemical characteristics of marine shale in the Wufeng Formation–Longmaxi Formation in the northern Sichuan Basin, South China and its implications for depositional controls on organic matter," *Journal of Petroleum Science and Engineering*, vol. 203, article 108618, 2021.

[4] J. Li, Q. Huang, G. Wang, E. Wang, S. Ju, and C. Qin, "Experimental study of effect of slickwater fracturing on coal pore structure and methane adsorption," *Energy*, vol. 239, article 122421, 2022.

[5] P. Zhao, L. Z. Xie, Z. C. Fan, L. Deng, and J. Liu, "Mutual interference of layer plane and natural fracture in the failure behavior of shale and the mechanism investigation," *Petroleum Science*, vol. 18, no. 2, pp. 618–640, 2021.

[6] Y. B. Liu, M. H. Li, G. Z. Yin, D. M. Zhang, and B. Z. Deng, "Permeability evolution of anthracite coal considering true triaxial stress conditions and structural anisotropy," *Journal of Natural Gas Science and Engineering*, vol. 52, pp. 492–506, 2018.

Downloaded from http://pubs.geoscienceworld.org/gsa/lithosphere/article-pdf/doi/10.2113/2022/9949201/5598962/9949201.pdf
by guest

[7] C. J. Fan, S. Li, M. K. Luo, W. Z. Du, and Z. H. Yang, "Coal and gas outburst dynamic system," *International Journal of Mining Science and Technology*, vol. 27, no. 1, pp. 49–55, 2017.

[8] M. Cheng, X. H. Fu, J. Q. Kang, Z. B. Tian, and Y. Y. Shen, "Experimental study on the change of the pore-fracture structure in mining-disturbed coal-series strata: an implication for CBM development in abandoned mines," *Energy & Fuels*, vol. 2, no. 35, pp. 1208–1218, 2020.

[9] J. Liu, L. Z. Xie, B. He, Q. Gan, and P. Zhao, "Influence of anisotropic and heterogeneous permeability coupled with in-situ stress on CO_2 sequestration with simultaneous enhanced gas recovery in shale: quantitative modeling and case study," *International Journal of Greenhouse Gas Control*, vol. 104, article 103208, 2021.

[10] P. Zhao, L. Z. Xie, B. He, and J. Liu, "Anisotropic permeability influencing the performance of free CH_4 and free CO_2 during the process of CO_2 sequestration and enhanced gas recovery (CS-EGR) from shale," *ACS Sustainable Chemistry & Engineering*, vol. 9, no. 2, pp. 914–926, 2021.

[11] H. H. Hou, G. D. Liang, L. Y. Shao, Y. Tang, and G. Y. Mu, "Coalbed methane enrichment model of low-rank coals in multi-coals superimposed regions: a case study in the middle section of southern Junggar Basin," *Frontiers of Earth Science*, vol. 15, no. 2, pp. 256–271, 2021.

[12] P. Zhang, D. F. Zhang, Y. Yang et al., "A case study on intergrated modeling of spatial information of a complex geological body," *Lithosphere*, vol. 2022, no. Special 10, 2022.

[13] Y. Wu, J. S. Liu, D. Elsworth, X. X. Miao, and X. B. Mao, "Development of anisotropic permeability during coalbed methane production," *Journal of Natural Gas Science and Engineering*, vol. 2, no. 4, pp. 197–210, 2010.

[14] F. G. Gu and R. Chalaturnyk, "Permeability and porosity models considering anisotropy and discontinuity of coalbeds and application in coupled simulation," *Journal of Petroleum Science and Engineering*, vol. 74, no. 3-4, pp. 113–131, 2010.

[15] C. Zhang, Q. S. Bai, and Y. H. Chen, "Using stress path-dependent permeability law to evaluate permeability enhancement and coalbed methane flow in protected coal seam: a case study," *Geomechanics and Geophysics for Geo-Energy and Geo-Resources*, vol. 6, no. 3, pp. 1–25, 2020.

[16] D. S. Yang, X. Y. Qi, W. Z. Chen, S. G. Wang, and F. Dai, "Numerical investigation on the coupled gas-solid behavior of coal using an improved anisotropic permeability model," *Journal of Natural Gas Science and Engineering*, vol. 34, pp. 226–235, 2016.

[17] W. Z. Cao, Q. H. Lei, and W. Cai, "Stress-dependent deformation and permeability of a fractured coal subject to excavation-related loading paths," *Rock Mechanics and Rock Engineering*, vol. 8, no. 54, pp. 4299–4320, 2021.

[18] Y. L. Tan, Z. J. Pan, J. S. Liu et al., "Experimental study of impact of anisotropy and heterogeneity on gas flow in coal. Part II: permeability," *Fuel*, vol. 230, pp. 397–409, 2018.

[19] H. Agheshlui, "Stress influence on the permeability of a sample heterogeneous rock," *Geomechanics and Geophysics for Geo-Energy and Geo-Resources*, vol. 5, no. 2, pp. 159–170, 2019.

[20] B. Q. Lin, H. R. Song, Y. Zhao, T. Liu, J. Kong, and Z. B. Huang, "Significance of gas flow in anisotropic coal seams to underground gas drainage," *Journal of Petroleum Science and Engineering*, vol. 180, pp. 808–819, 2019.

[21] Y. Ma, Z. J. Pan, N. N. Zhong et al., "Experimental study of anisotropic gas permeability and its relationship with fracture structure of Longmaxi Shales, Sichuan Basin, China," *Fuel*, vol. 180, pp. 106–115, 2016.

[22] C. Fan, S. Li, D. Elsworth, J. Han, and Z. Yang, "Experimental investigation on dynamic strength and energy dissipation characteristics of gas outburst-prone coal," *Energy Science & Engineering*, vol. 4, no. 8, pp. 1015–1028, 2020.

[23] M. Li, G. Yin, J. Xu, W. Li, Z. Song, and C. Jiang, "A novel true triaxial apparatus to study the geomechanical and fluid flow aspects of energy exploitations in geological formations," *Rock Mechanics and Rock Engineering*, vol. 12, no. 49, pp. 4647–4659, 2016.

[24] M. H. Li, G. Z. Yin, J. Xu, J. Cao, and Z. L. Song, "Permeability evolution of shale under anisotropic true triaxial stress conditions," *International Journal of Coal Geology*, vol. 165, pp. 142–148, 2016.

[25] C. Liu, G. Z. Yin, M. H. Li et al., "Shale permeability model considering bedding effect under true triaxial stress conditions," *Journal of Natural Gas Science and Engineering*, vol. 68, article 102908, 2019.

[26] M. Duan, C. B. Jiang, Q. Gan, H. B. Zhao, Y. Yang, and Z. K. Li, "Study on permeability anisotropy of bedded coal under true triaxial stress and its application," *Transport in Porous Media*, vol. 3, no. 131, pp. 1007–1035, 2020.

[27] C. Liu, G. Z. Yin, M. H. Li, D. L. Shang, B. Z. Deng, and Z. L. Song, "Deformation and permeability evolution of coals considering the effect of beddings," *International Journal of Rock Mechanics and Mining Sciences*, vol. 117, pp. 49–62, 2019.

[28] J. Li, Q. Huang, G. Wang, and E. Wang, "Influence of active water on gas sorption and pore structure of coal," *Fuel*, vol. 310, article 122400, 2022.

[29] H. D. Chen, Y. P. Cheng, H. X. Zhou, and W. Li, "Damage and permeability development in coal during unloading," *Rock Mechanics and Rock Engineering*, vol. 6, no. 46, pp. 1377–1390, 2013.

[30] C. Zhu, M. Karakus, M. C. He et al., "Volumetric deformation and damage evolution of Tibet interbedded skarn under multistage constant-amplitude-cyclic loading," *International Journal of Rock Mechanics and Mining Sciences*, vol. 152, article 105066, 2022.

[31] Y. Wang, H. N. Yang, J. Q. Han, and C. Zhu, "Effect of rock bridge length on fracture and damage modelling in granite containing hole and fissures under cyclic uniaxial increasing-amplitude decreasing-frequency (CUIADF) loads," *International Journal of Fatigue*, vol. 158, article 106741, 2022.

[32] M. Z. Gao, J. Xie, Y. A. Gao et al., "Mechanical behavior of coal under different mining rates: a case study from laboratory experiments to field testing," *International Journal of Mining Science and Technology*, vol. 31, no. 5, pp. 825–841, 2021.

[33] M. Z. Gao, J. Xie, J. Guo, Y. Q. Lu, Z. Q. He, and C. Li, "Fractal evolution and connectivity characteristics of mining-induced crack networks in coal masses at different depths," *Geomechanics and Geophysics for Geo-Energy and Geo-Resources*, vol. 7, no. 1, pp. 1–15, 2021.

[34] Z. Dou, Y. M. Liu, X. Y. Zhang et al., "Influence of layer transition zone on rainfall-induced instability of multilayered slope," *Lithosphere*, vol. 2021, article 2277284, no. Special 4, 2021.

[35] G. Li, Y. Hu, S. M. Tian, W. B. Ma, and H. L. Huang, "Analysis of deformation control mechanism of prestressed anchor on jointed soft rock in large cross-section tunnel," *Bulletin of*

Downloaded from http://pubs.geoscienceworld.org/gsa/lithosphere/article-pdf/doi/10.2113/2022/9949201/5598962/9949201.pdf
by guest

Engineering Geology and the Environment, vol. 12, no. 80, pp. 9089–9103, 2021.

[36] B. Zhao, G. C. Wen, J. Nian et al., "Numerical simulation study on the multi-physical field response to underground coal and gas outburst under high geo-stress conditions," *Minerals*, vol. 12, no. 2, p. 151, 2022.

[37] D. K. Wang, R. H. Lv, J. P. Wei et al., "An experimental study of seepage properties of gas-saturated coal under different loading conditions," *Energy Science & Engineering*, vol. 3, no. 7, pp. 799–808, 2019.

[38] K. Y. Tian and L. Qi, "Experimental study on gas seepage of bedded fractured coal body under stress loading and unloading," *Chinese Journal of Safety Science*, vol. 1, no. 27, pp. 93–97, 2017.

[39] M. K. Duan, C. B. Jiang, Q. Gan, M. H. Li, K. Peng, and W. Z. Zhang, "Experimental investigation on the permeability, acoustic emission and energy dissipation of coal under tiered cyclic unloading," *Journal of Natural Gas Science and Engineering*, vol. 73, article 103054, 2020.

[40] J. P. Zou, W. Z. Chen, D. S. Yang, H. D. Yu, and J. Q. Yuan, "The impact of effective stress and gas slippage on coal permeability under cyclic loading," *Journal of Natural Gas Science and Engineering*, vol. 31, pp. 236–248, 2016.

[41] Y. Q. Su, F. Q. Gong, S. Luo, and Z. X. Liu, "Experimental study on energy storage and dissipation characteristics of granite under two-dimensional compression with constant confining pressure," *Journal of Central South University*, vol. 28, no. 3, pp. 848–865, 2021.

[42] G. Bai, J. Su, Z. G. Zhang et al., "Effect of CO_2 injection on CH_4 desorption rate in poor permeability coal seams: an experimental study," *Energy*, vol. 238, article 121674, 2022.

[43] Y. H. Zhang, X. M. Xu, M. Lebedev, M. Sarmadivaleh, A. Barifcani, and S. Lglauer, "Multi-scale X-ray computed tomography analysis of coal microstructure and permeability changes as a function of effective stress," *International Journal of Coal Geology*, vol. 165, pp. 149–156, 2016.

[44] K. Wang, J. Zang, G. D. Wang, and A. Zhou, "Anisotropic permeability evolution of coal with effective stress variation and gas sorption: model development and analysis," *International Journal of Coal Geology*, vol. 130, pp. 53–65, 2014.

[45] C. J. Fan, H. O. Wen, S. Li, G. Bai, and L. J. Zhou, "Coal seam gas extraction by integrated drillings and punchings from the floor roadway considering hydraulic-mechanical coupling effect," *Geofluids*, vol. 2022, Article ID 5198227, 10 pages, 2022.

[46] Z. J. Wu, Z. Y. Wang, L. F. Fan, L. Weng, and Q. S. Liu, "Micro-failure process and failure mechanism of brittle rock under uniaxial compression using continuous real-time wave velocity measurement," *Journal of Central South University*, vol. 28, no. 2, pp. 556–571, 2021.

[47] Z. Dou, S. X. Tang, X. Y. Zhang et al., "Influence of shear displacement on fluid flow and solute transport in a 3D rough fracture," *Lithosphere*, vol. 2021, no. Special 4, article 1569736, 2021.

Downloaded from http://pubs.geoscienceworld.org/gsa/lithosphere/article-pdf/doi/10.2113/2022/9949201/5598962/9949201.pdf
by guest